

# Photoconductivity and diode effect in Bi rich multiferroic BiFeO<sub>3</sub> thin films grown by pulsed-laser deposition

K. Ahadi · S. M. Mahdavi · A. Nemati ·  
M. Kianinia

Received: 21 June 2010 / Accepted: 22 September 2010 / Published online: 4 November 2010  
© Springer Science+Business Media, LLC 2010

**Abstract** Bismuth ferrite, BiFeO<sub>3</sub>, is almost the only material that is simultaneously magnetic and a strong ferroelectric at room temperature. As a result it is the most investigated multiferroic material. In this study, bismuth ferrite thin films were deposited on silicon wafer (100) and glass by pulsed-laser deposition and their structural, optical, and electrical properties were measured. Our study indicates that Bi richness in these films can stimulate formation of oxygen vacancy in the system which in its turn leads to delocalization of carriers and a more intensified photoconductivity response. X-ray diffraction analysis revealed formation of BiFeO<sub>3</sub> (BFO), but it also showed formation of Bi<sub>2</sub>O<sub>3</sub> and Bi<sub>2</sub>O<sub>2.3</sub> as well as BFO. Energy dispersive spectrum (EDS) also showed higher atomic concentration of Bi with respect to Fe. It also disclosed Bi depletion through the films during post-growth heat treatment. Atomic force microscopy showed a homogeneous nano structure with columnar grains. It also disclosed that higher substrate temperature can improve smoothness of the films. Scanning electron microscopy depicted the thickness of about 200 nm. Transmission spectrum illustrated band gap of about 2 eV. Dark–light *IV* characteristics were conducted on the films which were subjected to

post-growth heat treatment at 0.01 and 760 Torr O<sub>2</sub>. Dark conductivities increased by an order of magnitude in comparison between films which were subjected to post-growth heat treatment at 0.01 and 760 Torr O<sub>2</sub>. Dark–light *IV* characteristics of the films also uncovered a remarkable increase in conductivity under illumination in comparison to dark one. Diode behavior of the films was investigated by *IV* characteristics as well.

## 1 Introduction

In the past few years, an immense research interest has been detected toward materials which show a concurrent magnetic and ferroelectric ordering [1, 2]. This is not the first time that such an interest has been observed. Such ‘magnetoelectric multiferroics’ were studied to some degree in the 1960s and 1970s [2] but then languished. This was mostly due to the lack of technology of producing single crystal magnetoelectric multiferroics in large scale at the time. Resurgence of magnetoelectric multiferroic materials has happened [2–4] first of all, because of high-quality single crystalline samples which lead to discovery of new types of multiferroics second, improved first-principle computational aiding techniques which helped to design new multiferroic materials with better coupling and higher magnetic and ferroelectric ordering and finally, advances in thin film deposition techniques which made possible producing some structures and phases that used to be inaccessible by conventional chemical routes. Coexistence of magnetism and ferroelectricity is a rare phenomenon mostly due to the known trend in magnetic materials to have a half filled d-band cation and being conductive and ferroelectrics’ tendency to have an empty d-band cation and being resistant [5]. Furthermore coexistence of magnetism and

---

K. Ahadi (✉) · A. Nemati · M. Kianinia  
Department of Materials Science and Engineering,  
Sharif University of Technology, P.O. Box 11155-9466,  
Azadi Ave., Tehran, Iran  
e-mail: ahadi\_kaveh@mehr.sharif.edu

S. M. Mahdavi  
Physics Department, Sharif University of Technology,  
P.O. Box 11365-9466, Azadi Ave., Tehran, Iran

S. M. Mahdavi  
Institute for Nanoscience and Nanotechnology, Sharif University  
of Technology, P.O. Box 14588-89694, Azadi Ave., Tehran, Iran

ferroelectricity cannot guarantee their strong coupling [2, 6] and in reality having these two contrasting phenomena will lead to the loss of strong bonding between them in a high amount. Multiferroic thin films have interesting properties and are stimulated by the potential applications in non-volatile ferroelectric memories and devices based on magnetoelectric effect [3]. Bismuth ferrite (BFO) is the most investigated multiferroic and a potentially important lead-free ferroelectric. BFO thin films have the potential to display a spontaneous polarization an order of magnitude higher than that of bulk by strain engineering [7]. It also shows the highest ferroelectric polarization, with a ferroelectric Curie temperature of ( $T_C$ ) 830 °C and an antiferromagnetic Néel temperature of ( $T_N$ ) 370 °C [8]. These high Curie and Néel temperatures become more and more interesting upon knowing that most of the magnetoelectric multiferroics have Curie and Néel temperatures under the room temperature which limits their application. Despite great interest in multiferroic thin films, there are only few studies regarding the photoconductivity and diode behavior in BFO [9–11]. These properties and the optical band gap in BiFeO<sub>3</sub> are interesting, due to its potential applications in the field of spintronic, optoelectronic, and magneto-optical device.

## 2 Experimental procedure

Thin films of bismuth ferrite were deposited using pulsed-laser deposition (PLD) technique with a (MPB, ASX-750) KrF (248 nm) excimer laser. 5,000 pulses with 10 Hz frequency were applied. Substrate–target distance was fixed at 6.5 cm. Before deposition, chamber was pumped to  $5 \times 10^{-6}$  Torr and then by flowing pure O<sub>2</sub>, partial pressure of oxygen ( $P_{O_2}$ ) was controlled and stabilized at 100 mTorr during ablation. N type silicon wafer (100) and glass were utilized as substrate. A mixture of Fe<sub>2</sub>O<sub>3</sub> and Bi<sub>2</sub>O<sub>3</sub> powders was used as target. The atomic concentration ratio of Bi/Fe of 60/40 (T6) was used in target. T6 films were deposited at 300 and 550 °C and then T6.300 films were subjected to heat treatment at 650 °C for 1 h in an oxygen-rich atmosphere (T6.300h). The PLD processing detail is presented in Table 1.

X-ray diffraction (XRD, Siemens D/5000) Cu K $\alpha$  was used to study phase analysis of the T6.300 and T6.550 films. It also was used to investigate phase transformation on target surface before and after target–laser interaction. XRD analysis was obtained by an X'pert (PANalytical High Score). Energy dispersive spectrum (EDS) was also used to study atomic concentration ratio of Bi to Fe. The surface topography of the thin films deposited at different temperatures and before and after heat treatment was studied by a Thermo Microscopes Autoprobe CP-Research atomic force microscopy (AFM) in air with a silicon tip

**Table 1** PLD processing details of T6.300, T6.300h, and T6.550 films

	Substrate temperature (°C)	Bi/Fe atomic ratio of target	O <sub>2</sub> partial pressure (mTorr)	Deposition rate (nm/min)	Energy density (J/cm <sup>2</sup> )
T6.300	300	1.5	100	20	1
T6.300h	300	1.5	100	20	1
T6.550	550	1.5	100	20	1

with radius of 10 nm and in contact mode. Scanning electron microscopy (SEM, Vega© Tescan) was utilized to study the thickness and the microstructure of the thin films and the target before and after processing. Spectrophotometer analysis (Elmer Perkin Lambda 20) was also used from 200 to 1,100 nm with scan rate of 10 nm/s. The data used to study the transmittance behavior and band gap of the thin films. Dark–light *IV* characteristics of the films were measured in darkness and illumination of 100 mW/cm<sup>2</sup> white light source, peaked around 550 nm, to investigate photoconductivity and diode behavior of the films.

## 3 Results and discussion

Figure 1a and b shows SEM micrographs of the target before and after PLD processing respectively. The microstructure had experienced an immense growth which might be attributed to high local temperature during laser–target interaction. As it can be inferred from Z-contrast, Fe<sub>2</sub>O<sub>3</sub> particles stand rigidly between molten and solidified Bi<sub>2</sub>O<sub>3</sub> particles. This is exactly due to lower melting point of Bi<sub>2</sub>O<sub>3</sub>. A crack in Fig. 1b is distinguishable which can be related to shrinkage during solidification of Bi<sub>2</sub>O<sub>3</sub> particles. Figure 2 shows XRD pattern of the target before and after processing. It clarifies presence of just Bi<sub>2</sub>O<sub>3</sub> and Fe<sub>2</sub>O<sub>3</sub> phases and formation of no other phase during PLD processing. The peaks of Bi<sub>2</sub>O<sub>3</sub> and Fe<sub>2</sub>O<sub>3</sub> in Fig. 2 are consistent with 00-001-0709 and 01-073-0603 reference numbers respectively. According to 00-001-0709 reference card number, Bi<sub>2</sub>O<sub>3</sub> has the main  $2\theta$  peak at 27.4° which is in accordance with Fig. 2. According to 01-073-0603 reference card number, Fe<sub>2</sub>O<sub>3</sub> has the main  $2\theta$  peak at 35.6° which is again in accordance with Fig. 2. The noteworthy reduction in the intensity of the XRD pattern after PLD processing might be related to the rapid melting and solidification on the surface of the target which lead to loss of crystalline characteristics to a high amount.

Based on XRD studies, T6.300 film did not show any special peak which may be attributed to low substrate temperature during deposition. XRD pattern of T6.550h film is presented in Fig. 3 and peaks from BiFeO<sub>3</sub>, Bi<sub>2</sub>O<sub>3</sub>,

**Fig. 1** SEM images of target **a** before and **b** after PLD processing

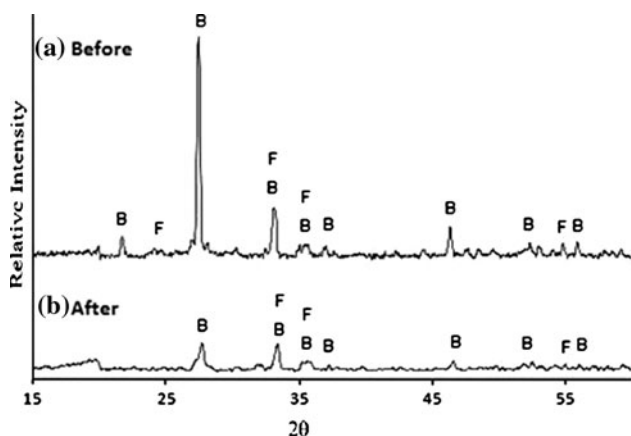
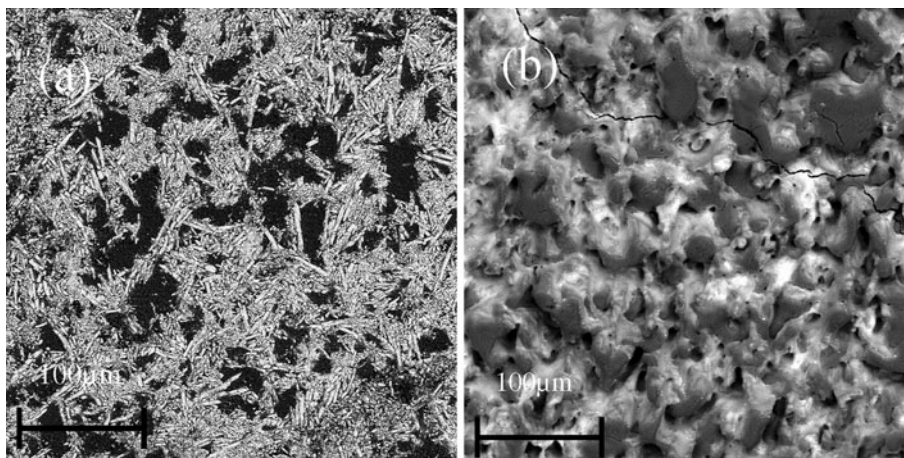


**Fig. 2** XRD analysis of target **a** before and **b** after PLD processing (B and F stand for  $\text{Bi}_2\text{O}_3$  and  $\text{Fe}_2\text{O}_3$  phases respectively)

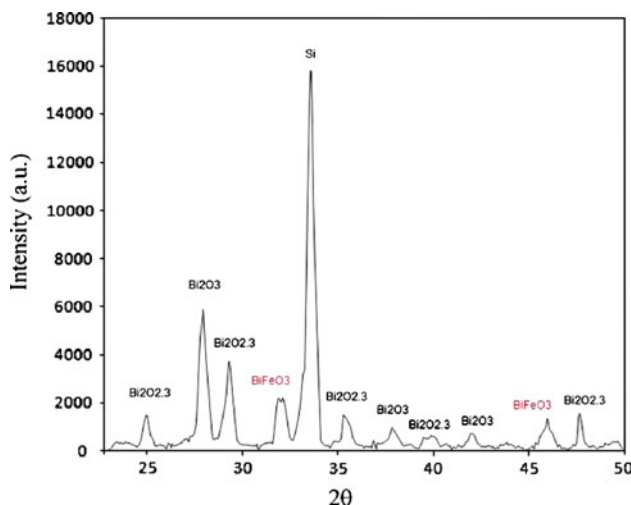


**Fig. 3** XRD pattern of T6.550 film deposited on silicon wafer (100) at 100 mTorr  $\text{O}_2$

$\text{Bi}_2\text{O}_{2.3}$ , and Si can be distinguished. Formation of  $\text{Bi}_2\text{O}_3$  and  $\text{Bi}_2\text{O}_{2.3}$  as it has been reported may be related to over stoichiometry of Bi in the film [12]. The peaks of  $\text{Bi}_2\text{O}_3$

and  $\text{Bi}_2\text{O}_{2.3}$  in Fig. 3 are consistent with 00-018-0244 and 00-027-0051 reference card numbers respectively. According to mentioned reference card numbers  $\text{Bi}_2\text{O}_3$  and  $\text{Bi}_2\text{O}_{2.3}$  share a peak around  $33^\circ$ . These peaks correlate with strong peak of substrate. Again according to mentioned reference card numbers  $\text{Bi}_2\text{O}_3$  and  $\text{Bi}_2\text{O}_{2.3}$  have their main  $2\theta$  peaks at  $28.4^\circ$  and  $29.2^\circ$ . EDS showed that the atomic concentration ratio of Bi/Fe was 2.91 for T6.550 film. According to 01-071-2494 reference code, BFO has a doublet peak around  $31.8^\circ$  which both are almost the main peaks. At last according to 01-080-0018 reference code for Si, (200) planes'  $2\theta$  peak would be at  $33.2^\circ$  which is in accordance with Fig. 3. Formation of  $\text{Bi}_2\text{SiO}_5$  was previously reported by Wang and Nan [13] which were attributed to higher diffusion rate of iron atoms. Iron atoms during heat treatment diffuse up and let Bi, Si, and O atoms to form a thin in situ buffer layer, which relaxes epitaxial strain. Formation of  $\text{Bi}_2\text{SiO}_5$  was not presented by XRD pattern, which may again be related to Bi over stoichiometry in the system.

Figure 4a–c shows energy dispersive spectra of T6.300, T6.300h, and T6.550 films respectively. EDS results demonstrated Bi/Fe atomic concentration ratios of 3.21 for T6.300 and 1.43 for T6.300h films. Higher atomic concentration of Bi in the films with respect to target may be attributed to high equilibrium vapor pressure of Bi, which makes desorption of Bi atoms easier to both surface of the target and thin film than that of Fe atoms. In fact, volatility of Bi is one of the main factors that should be considered in the deposition of BFO by PLD. This volatility helps the depletion of Bi during the heat treatment of the films [12].

Figure 5a–c shows AFM images of T6.300, T6.300h, and T6.550 films respectively. Table 2 shows the average grain size, average roughness ( $R_a$ ) and rms roughness ( $R_q$ ) of the films. According to micrographs, grains' growth is columnar, with a rather homogeneous distribution of the size, and with no apparent fault. A remarkable increase in grain size has been detected in T6.300 film after heat

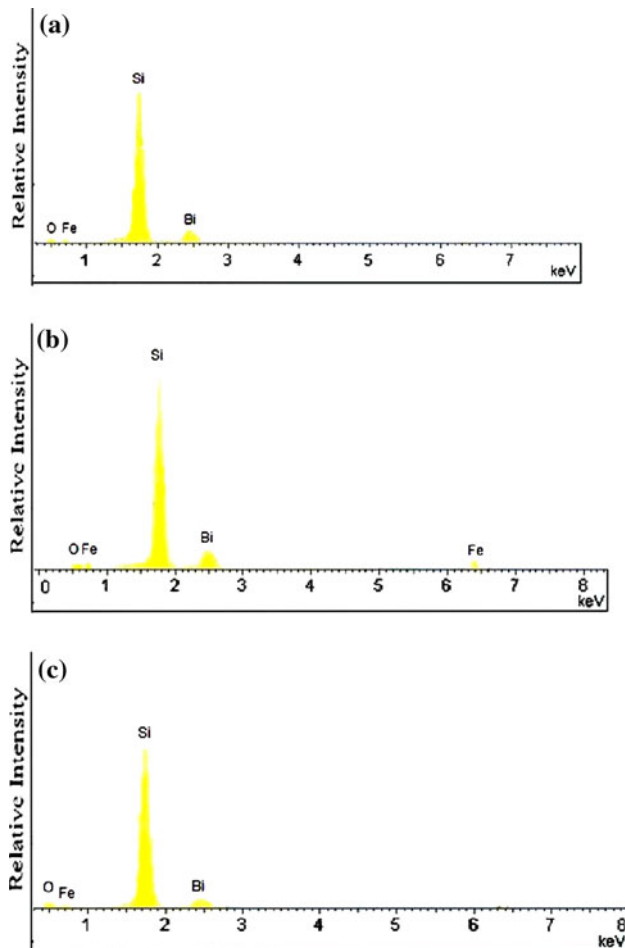


**Fig. 4** a–c Energy dispersive spectra of T6.300, T6.300h, and T6.550 films respectively

treatment which was expected. Comparison between T6.300 and T6.550 revealed that substrate temperature has no noticeable effect on grain size, but has a tremendous effect on roughness of the films. Higher substrate temperature can enhance smoothness of the films [14]. This higher smoothness is due to inter layer diffusion of atoms during film deposition.

The microstructure of the thin films was characterized through SEM. As shown in Fig. 6a T6.300 film is dense,

**Fig. 5** a–c AFM images of T6.300, T6.300h, and T6.600 films respectively

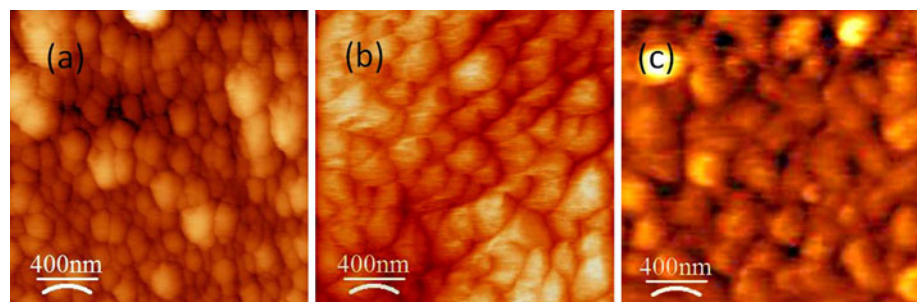


**Table 2** Average grain size, average roughness ( $R_a$ ), and rms roughness ( $R_q$ ) of the T6.300, T6.300h, and T6.550 films

	Average grain size (nm)	Centre line average roughness, $R_a$ (nm)	Rms average roughness, $R_q$ (nm)
T6.300	100 ± 33	15.95 ± 1.24	20.27 ± 1.87
T6.300h	184 ± 64	19.62 ± 1.38	24.44 ± 2.02
T6.550	107 ± 29	2.120 ± 0.43	3.179 ± 0.54

smooth, and homogeneously grown with most of the grains smaller than 100 nm. The cross-section SEM image in Fig. 6b shows a thickness of about 200 nm for T6.300 film.

Spectrophotometer analysis was used to study the transmittance behavior of the T6.300 film, deposited on glass. Band gap has been calculated from the classical equation:

$$(\alpha hv) = A(hv - E_g)^\eta \quad (1)$$

where  $\alpha$  is the linear absorption coefficient,  $E_g$  is the band gap energy,  $A$  is a constant,  $hv$  is the photon energy, and  $\eta$  is a constant which is equal to 0.5 and 2 for direct and indirect band gap materials. Figure 7 shows that the material has a direct band gap as it has been reported earlier [15, 16]. Direct band gap of 2 eV has been determined for T6.300 films. However, the onset of absorption was about 1.2 eV. An onset with lower energy than band gap was previously reported by Basu et al. too [9].

Dark–light  $IV$  characteristics of the T6.300 films, deposited on glass and heat treated at different atmospheres, were measured. The aim was to investigate both whether there is any change in conductivity under illumination symmetry of the  $IV$  diagram. The enhancement in conductivity under illumination is attributed to photo-excited carriers driven by the polarization. In the other hand the symmetry of the diagram is applied to study diode behavior of the films.

Under illumination with wavelength equal to or larger than the band gap, the photo-excited carriers will add up to dark ones and a larger current is expected. This can be expressed by the following equation which is common for ferroelectric materials.

**Fig. 6** SEM images of T6.300 film **a** surface of the film and **b** cross-section image of the film

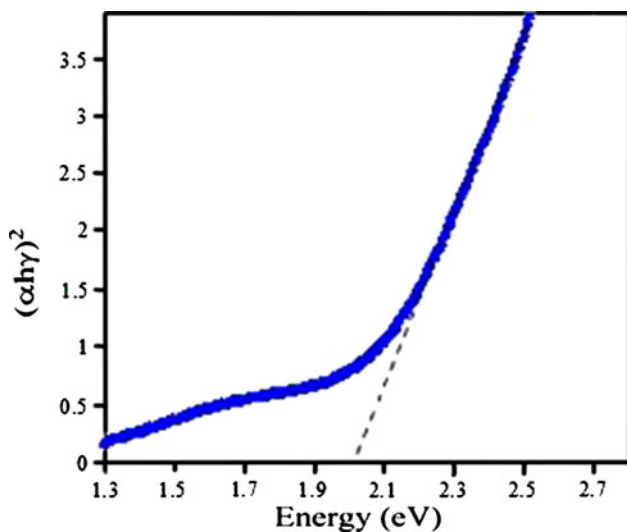
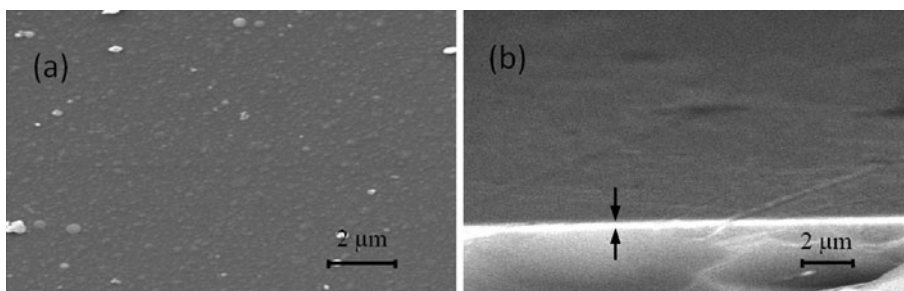


**Fig. 7**  $(\alpha hv)^2$  versus energy for T6.300 thin film. Dashed lines indicate an extrapolation for determination of the band gap  $E_g$

$$J = (\sigma_d + \sigma_{ph})E \tag{2}$$

where  $\sigma_d$  and  $\sigma_{ph}$  are dark and light component of conduction respectively. With light illumination peaked around 550 nm (about 2.3 eV), which is larger than optical band gap of the films, excitation of carriers is expected. Figure 8 shows *IV* characteristics of the T6.300h films at the same heat treatment cycle and just at different atmospheres. In both films a remarkable enhancement in conductivity is evident under illumination in the first quadrant. To avoid any Schottky barrier, FTO were used as both top and bottom electrodes.

As we know, presence of oxygen vacancies can insert electrons into the structure and boost free-carrier concentration. With heat treatment at 760 Torr of  $O_2$  partial pressure no noticeable oxygen vacancy will remain in the system. In contrary, a remarkable enhancement in the conductivity of the film is detectable; a result that has not been reported earlier [9]. Therefore, there must be another source for oxygen vacancy. This source might be related to Bi over stoichiometry and is investigated by defect chemistry. The defect chemistry in Bi over stoichiometry BFO

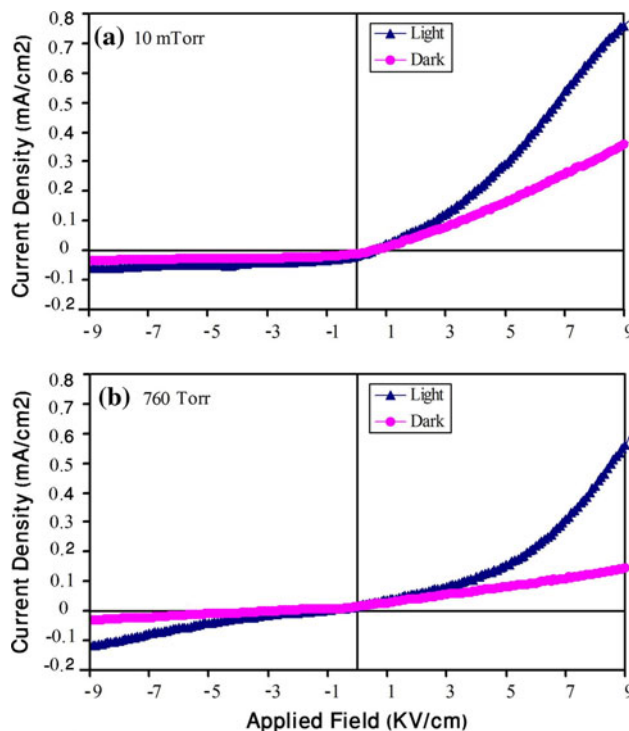
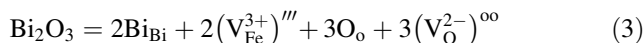
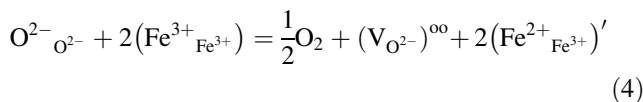


**Fig. 8** Dark–light *IV* characteristics of the T6.300 films which were heat treated at **a** 10 mTorr and **b** 760 mTorr  $O_2$

can be expressed by using Kröger–Vink notation as following:



With heat treatment at 10 mTorr  $O_2$  partial pressure, oxygen vacancies were introduced into the lattice. This new type of vacancy adds up to the former one. The new type of oxygen vacancy was proposed by Basu et al. [9] as the following defect chemistry relationship:



In previous studies large leakage currents in BFO were typically attributed to the presence of oxygen vacancies [17]. It seems to us that, by using above defect chemistry, electrons can hop from  $Fe^{2+}$  to adjacent  $Fe^{3+}$  ions through

oxygen centers. For further support, Pabst et al. recently identified Poole–Frenkel conduction as being the dominant leakage mechanism in BFO thin films [18].

At an applied field of 10 kV/cm dark conductivities of 1.7 and  $3.9 \times 10^{-8} \Omega^{-1} \text{cm}^{-1}$  were measured for films heat treated in 760 and 0.01 Torr. At the same applied field of 10 kV/cm illuminated conductivities of  $5.6 \times 10^{-7}$  and  $1.0 \times 10^{-5} \Omega^{-1} \text{cm}^{-1}$  were measured for films heat treated in 760 and 0.01 Torr  $\text{O}_2$ . Formation of Bi rich phases can amplify band gap in BFO. Ahadi et al. previously showed that optical band gap of the BFO films increases remarkably with increase of Bi content of the films [19].

First and third quadrants of *IV* diagram in Fig. 7a and b are asymmetrical and show a diode behavior. This may be attributed to distribution of oxygen vacancies in the film which perform as an inherent p–n junction [20]. If this supposition is true, then the behavior must be switchable by reversing permanent spontaneous polarization in the films. Switchable diode effect in BFO has also been reported by Choi et al. [10].

#### 4 Conclusion

In summary, Bi rich  $\text{BiFeO}_3$  thin films were obtained with a homogenous nano structure via pulsed-laser deposition method. Formation of  $\text{BiFeO}_3$ ,  $\text{Bi}_2\text{O}_3$ , and  $\text{Bi}_2\text{O}_{2.3}$  in the films was proven by XRD analysis. EDS analysis also verified Bi abundance in the films and Bi depletion during post-growth heat treatment to a high amount as well. The onset of absorption was at 1.2 eV and the direct band gap energy was 2 eV for the films. Dark *IV* characteristics of the films subjected to post-growth heat treatment at 0.01 Torr  $\text{O}_2$  showed an immense increase which was attributed to oxygen vacancies. It was shown that Bi richness can also induce oxygen vacancy into the lattice and can improve electrical conductivity and photoconductivity effect of the films. Dark–light *IV* characteristics of the films also uncovered diode behavior of the thin films.

**Acknowledgments** The authors acknowledge the Research and Development Deputy of Sharif University of Technology for supporting this work. This work was also supported and funded by Iranian Nanotechnology Initiative Council. The authors also would like to acknowledge Mr. Mohammad Reza Nematollahi, Mr. Farhang Parsikia, Ms. Elham Nemati and Dr. Mehdi Ranjbar for their helps.

#### References

1. W. Eerenstein, N.D. Mathur, J.F. Scott, *Nature* **442**, 759 (2006). doi:[10.1038/nature05023](https://doi.org/10.1038/nature05023) (review)
2. R. Ramesh, N.A. Spaldin, *Nat. Mater.* **6**, 21 (2007). doi:[10.1038/nmat1805](https://doi.org/10.1038/nmat1805) (review)
3. N.A. Spaldin, M. Fiebig, *Science* **309**, 391 (2005). doi:[10.1126/science.1113357](https://doi.org/10.1126/science.1113357)
4. M. Fiebig, *J. Phys. D* **38**, R123 (2005). doi:[10.1088/0022-3727/38/8/R01](https://doi.org/10.1088/0022-3727/38/8/R01)
5. N.A. Hill, *J. Phys. Chem. B* **104**, 6694 (2000). doi:[10.1021/jp000114x](https://doi.org/10.1021/jp000114x)
6. S.W. Cheong, M. Mostovoy, *Nat. Mater.* **6**, 13 (2007). doi:[10.1038/nmat1804](https://doi.org/10.1038/nmat1804)
7. J. Wang, J.B. Neaton, H. Zheng, V. Nagarajan, S.B. Ogale, B. Liu, D. Viehland, V. Vaithyanathan, D.G. Schlom, U.V. Waghmare, N.A. Spaldin, K.M. Rabe, M. Wuttig, R. Ramesh, *Science* **299**, 1719 (2003). doi:[10.1126/science.1080615](https://doi.org/10.1126/science.1080615)
8. Y.H. Chu, L.W. Martin, M.B. Holcomb, M. Gajek, S.J. Han, Q. He, N. Balke, C.H. Yang, D. Lee, W. Hu, Q. Zhan, P.L. Yang, A.F. Rodríguez, A. Scholl, S.X. Wang, R. Ramesh, *Nat. Mater.* **7**, 478 (2008). doi:[10.1038/nmat2184](https://doi.org/10.1038/nmat2184)
9. S.R. Basu, L.W. Martin, Y.H. Chu, M. Gajek, R. Ramesh, R.C. Rai, X. Xu, J.L. Musfeldt, *Appl. Phys. Lett.* **92**, 091905 (2008). doi:[10.1063/1.2887908](https://doi.org/10.1063/1.2887908). (3 p)
10. T. Choi, S. Lee, Y.J. Choi, V. Kiryukhin, S.W. Cheong, *Science* **324**, 63 (2009). doi:[10.1126/science.1168636](https://doi.org/10.1126/science.1168636)
11. S.Y. Yang, L.W. Martin, S.J. Byrnes, T.E. Conry, S.R. Basu, D. Paran, L. Reichertz, J. Ihlefeld, C. Adamo, A. Melville, Y.H. Chu, C.H. Yang, J.L. Musfeldt, D.G. Schlom, J.W. Ager, R. Ramesh, *Appl. Phys. Lett.* **95**, 062909 (2009). doi:[10.1063/1.3204695](https://doi.org/10.1063/1.3204695). (3 p)
12. L. Bi, A.R. Taussig, H.S. Kim, L. Wang, G.F. Dionne, D. Bono, K. Persson, G. Ceder, C.A. Ross, *Phys. Rev. B* **78**, 104 (2008). doi:[10.1103/PhysRevB.78.104106](https://doi.org/10.1103/PhysRevB.78.104106)
13. Y. Wang, C.W. Nan, *Thin Solid Films* **517**, 4484 (2009). doi:[10.1016/j.tsf.2009.02.142](https://doi.org/10.1016/j.tsf.2009.02.142)
14. H.M. Christen, G. Eres, *J. Phys.: Condens. Matter* **20**, 264005 (2008). doi:[10.1088/0953-8984/20/26/264005](https://doi.org/10.1088/0953-8984/20/26/264005)
15. Y. Xu, M. Shen, *Mater. Lett.* **62**, 3600 (2008). doi:[10.1016/j.matlet.2008.04.006](https://doi.org/10.1016/j.matlet.2008.04.006)
16. S.J. Clark, J. Robertson, *Appl. Phys. Lett.* **90**, 132903 (2007). doi:[10.1063/1.2716868](https://doi.org/10.1063/1.2716868). (3 p)
17. Y.P. Wang, L. Zhou, M.F. Zhang, X.Y. Chen, J.M. Liu, Z. Liu, *Appl. Phys. Lett.* **84**, 1731 (2004). doi:[10.1063/1.1667612](https://doi.org/10.1063/1.1667612). (3 p)
18. G.W. Pabst, L.W. Martin, Y.H. Chu, R. Ramesh, *Appl. Phys. Lett.* **90**, 072902 (2007). doi:[10.1063/1.2535663](https://doi.org/10.1063/1.2535663). (3 p)
19. K. Ahadi, A. Nemati, S.M. Mahdavi, M. Nematollahi, M. Ranjbar, Optical Properties of Bi Rich Multiferroic  $\text{BiFeO}_3$  Thin Films Grown by Pulsed Laser Deposition, in *Proceedings of International Conference on Nanotechnology: Fundamentals and Applications*, Ottawa, Ontario, Canada, 4–6 August 2010, paper no. 389
20. C.H. Yang, J. Seide, S.Y. Kim, P.B. Rossen, P. Yu, M. Gajek, Y.H. Chu, L.W. Martin, M.B. Holcomb, Q. He, P. Maksymovych, N. Balke, S.V. Kalinin, A.P. Baddorf, S.R. Basu, M.L. Scullin, R. Ramesh, *Nat. Mater.* **8**, 485 (2009). doi:[10.1038/NMAT2432](https://doi.org/10.1038/NMAT2432)